



Exploring a novel chamfered tool design for short duration refill friction stir spot welds of high strength aluminium

Jonathan Draper¹ · Sebastian Fritsche² · Sergio de Traglia Amancio-Filho² · Alexander Galloway¹ · Athanasios Toumpis¹

Received: 16 October 2023 / Accepted: 20 February 2024 / Published online: 5 March 2024
© The Author(s) 2024

Abstract

This work investigates refill friction stir spot welded joints of AA2024-T3 aluminium alloy, produced with short welding times between 3 s and 0.75 s. A novel tool geometry that incorporates a chamfer on the inner edge of the shoulder tip is investigated as a means of improving joint quality at short welding times by easing material flow during the refill stage. The influence of shoulder design on weld microstructure, defect formation, material flow, and mechanical properties was assessed. When compared with a standard shoulder geometry, it was found that the introduction of a chamfer on the inner tip edge improved material flow during the refill stage and led to improved material mixing at the weld periphery. The formation of voids in the region of the weld periphery was eliminated and tensile lap-shear strength of the welded joints was increased by 19% to 7.2 kN, and 27% to 8.16 kN, for 0.75 s and 1.5 s duration welds, respectively.

Keywords Refill Friction Stir Spot Welding · Aluminium alloys · Tool geometry · Solid-state joining · AA2024-T3

1 Introduction

Refill friction stir spot welding (RFSSW) is a solid-state spot welding technique that is well suited to lap joining of thin aluminium sheets, and offers a lightweight, durable alternative to mechanical fasteners [1, 2]. It is also capable of joining high strength aluminium such as 2xxx and 7xxx series alloys that are prone to hot cracking during fusion based spot welding processes (arc, resistance, laser) [3, 4]. As illustrated in Fig. 1, the RFSSW process uses a tool comprised of three parts assembled axially concentric. During the clamping stage, the clamping ring secures the workpiece by applying a downward force; it then remains stationary for the remainder of the process. Within the clamping ring, the shoulder and pin rotate complimentary with one another. During the plunging stage, the shoulder moves downwards and plunges into the workpiece, heating, and displacing

material while the pin simultaneously retracts upwards to provide a cavity for the displaced material to flow into. The shoulder and pin then return to their original positions during the refill stage, extruding the displaced material back into the weld and leaving a flat workpiece surface.

The micrograph shown in Fig. 2 highlights several key regions of a RFSSW joint: the stir zone (SZ), the thermomechanically affected zone (TMAZ), and the heat affected zone (HAZ). The SZ is the region of the weld within the outer bounds of the shoulder plunge path where material is stirred by the welding tool. High temperature and plastic deformation result in full or partial dynamic recrystallization within the SZ, leading to highly refined, equiaxed grain structures [5–7], although coarser grains can sometimes be found in the weld centre, where plastic deformation is less extreme [8]. The TMAZ begins at the periphery of the shoulder plunge path. Temperature is high in this region due to the proximity of the rotating shoulder, but deformation is moderate compared with the SZ. The resulting grains are distorted and elongated in the direction of the shoulder rotation but dynamic recrystallisation does not occur [6]. The HAZ experiences no plastic deformation and is only influenced by the thermal cycle of the welding process, causing grain and precipitate coarsening [6, 9].

A significant amount of research has been carried out focusing on optimising the key welding parameters of tool

✉ Jonathan Draper
jonathan.draper@strath.ac.uk

¹ Department of Mechanical & Aerospace Engineering, University of Strathclyde, Glasgow, UK

² Institute of Materials Science, Joining and Forming, Graz University of Technology, BMK Endowed Professorship for Aviation, Graz, Austria

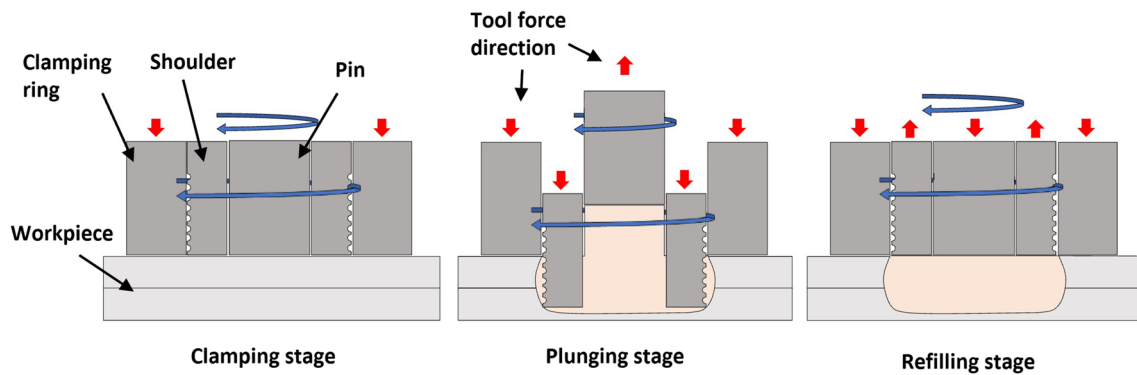


Fig. 1 Stages of the refill friction stir spot welding process

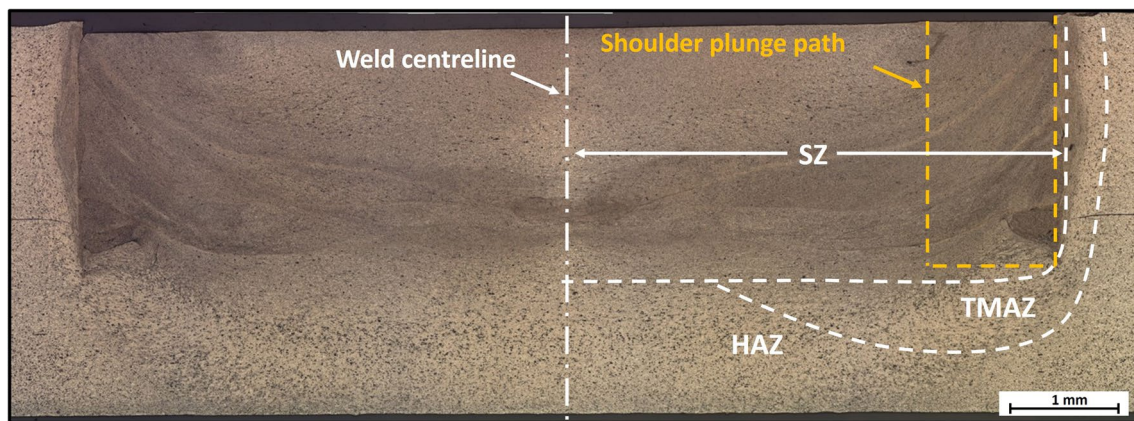


Fig. 2 Reference weld produced with a standard shoulder using optimised parameters from [10] (2310 rpm rotational speed, 2.25 mm plunge depth, 5.3 s welding time)

rotational speed, tool plunge depth, and welding time, as reviewed elsewhere [11, 12]. The majority of the published work has sought to maximise weld strength, which is generally achieved with weld times longer than 4 s. As competitor technologies such as resistance spot welding can produce joints in 1–2 s [13], the duration of the RFSSW process will need to be reduced if it is to be considered a viable alternative for mass manufacturing applications [12]. Although comparable welding times (<2 s) have been successfully employed for 5xxx and 6xxx series aluminium [9, 14–16], this has not been widely reported on for high strength aluminium alloys such as AA2024-T3. Several studies have achieved high quality AA2024 joints, although at the cost of welding times in excess of 5 s [5, 10, 17].

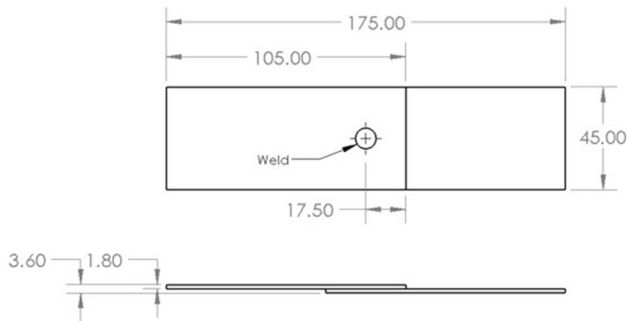
A potential solution to this challenge that remains to be fully explored is that of alternative welding tool geometries. This involves modifying the shape of the shoulder or pin tip to enhance material flow, improve mixing, or influence heat generation during the welding process. Multiple studies by Łogin et al. [18, 19] reported on the influence of various clockwise and counter-clockwise

grooves on shoulder end-faces to improve the distribution of alclad coating when joining AA2024-T3 sheets. An increase in ultimate lap-shear force (ULSF) of 15% was achieved with a spiral grooved end-face at a welding time of 4 s. This improvement was attributed to enhanced mixing of the alclad layer. A number of studies by Shen et al. [20–22] investigated a grooved shoulder end-face to improve mixing between dissimilar aluminium sheets. The authors found that the presence of grooves reduced defects within the weld and increased lap-shear strength, although only 5 s weld times were considered. Li et al. [23] investigated three shoulder variants to join 2A12-T42 aluminium sheets; a smooth outer surface and end-face, a threaded outer surface with grooved end-face, and a smooth outer surface with grooved end-face. Both thread and groove modifications increased material mixing, and the highest ULSF of ≈ 10 kN was achieved with the grooved shoulder, although only very long welds of 12 s were studied.

The current work is an investigation of welds produced at much shorter welding times than previously reported in the literature for AA2024-T3. Welding times as low as 0.75 s

Table 1 Chemical composition [25] and mechanical properties of AA2024-T3

Chemical composition (wt%)										Mechanical properties		
Al	Si	Fe	Cu	Mn	Mg	Cr	Ni	Zn	Ti	Tensile strength (MPa)	Yield strength (MPa)	Elongation (%)
Bal	0.5	0.5	4.9	0.9	1.8	0.1	0.05	0.25	0.15	509	375.8	13.9

**Fig. 3** Dimensions and configuration of welding samples

are explored with the aim of increasing the applicability of RFSSW to high production rate environments. To address issues relating to poor material flowability at short welding times, this study explores an innovative new design for the shoulder component of the tool. The novel shoulder incorporates a chamfered tip (Section 2.1) to improve material flow during the refill stage and improve mechanical properties of the welds.

2 Materials and methods

The material investigated in this study was aluminium alloy AA2024-T3. The composition and mechanical properties of the base material are given in Table 1. Mechanical properties were established through pure tensile testing in accordance with BS EN ISO 6892-1:2019 [24], using an Instron 5969 universal testing machine.

Lap-shear joint specimens of 1.8 mm thick AA2024-T3 sheets were manufactured in the configuration shown in Fig. 3 using an RPS100 RFSSW machine (Harms & Wende).

2.1 Modified tool geometry

Welds were produced using two different shoulder geometries: a conventional cylindrical design with an external thread (Fig. 4a), and a novel design with a 45° chamfer on the inner rim, leaving a 0.7 mm wide end-face (Fig. 4b). Both shoulder geometries had inner and outer diameters of 6.4 mm and 9 mm, respectively. The clamping ring outer diameter was 18 mm.

Joints were produced at welding times of 3 s, 1.5 s and 0.75 s. The maximum welding time of 3 s, and a rotational speed of 1500 rpm, were selected to match the shortest welding time previously reported in the literature [26]. The minimum welding time of 0.75 s was dictated by the limitations of the welding equipment. Shoulder plunge depth was kept at 1.25 times the top sheet thickness, in line with the optimal plunge depth most often identified in the literature [27, 28]. Volume ratio (ratio of shoulder plunge volume to pin retraction volume) was kept constant at 0.8. Parameters for all of the welds produced are given in Table 2.

Samples were sectioned through the weld centre and prepared to a final polish with 0.02 μm OPS using a standard metallographic preparation process, and electro-etched using Barker's solution (20 ml HBF₄, 80 ml H₂O) for 120 s. Weld microstructures were characterised using an Olympus GX51 metallurgical microscope. Fractography was performed using a HITACHI SU-6600 scanning electron microscope (SEM).

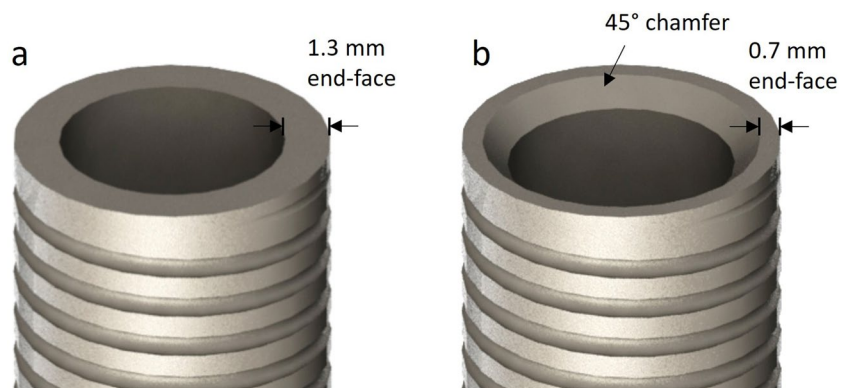
Fig. 4 Shoulder geometries **a)** standard shoulder, **b)** chamfered shoulder

Table 2 Welding parameters for all tested specimens

Parameter ID	Shoulder	Welding time (s)	Rotational speed (rpm)	Plunge depth (mm)	Volume ratio
01	Standard	3	1500	2.25	0.8
02		1.5			
03		0.75			
04	Chamfered	3	1500	2.25	0.8
05		1.5			
06		0.75			

To establish the influence of shoulder geometry on hardness throughout the weld region, Vickers HV0.05 microhardness maps were produced using a Qness 60 A + Evo hardness tester (QATM), in accordance with BS EN ISO 6507–4:2018 [29]. Measurements were taken in a square grid pattern with a spacing of 0.1 mm and dwell time of 10 s. ULSF was determined via tensile lap-shear testing using an Instron 5969 universal testing machine, with a crosshead speed of 2 mm/min, in accordance with EN ISO 14273. An average ULSF was calculated from 3 replicants of each welding condition.

3 Results and discussion

3.1 Weld macrostructure

Figure 5 presents macrographs of welds produced using each shoulder variant and reveals several significant differences in hook geometry, void formation, and extent of mixing at the lap interface and SZ/TMAZ interface.

3.1.1 Hook morphology

The hook defect forms at the transition from welded to un-welded material, where the plunging motion of the shoulder plastically deforms the seam of the top and bottom sheet into a downwards sloping hook. The hook acts as a stress concentrator and point of crack initiation; larger hook heights have been shown to amplify this effect and reduce ULSF [6, 8, 16, 30]. Figure 5a–c shows that the standard shoulder produced downwards sloping hooks at all weld times, with hook height decreasing with shorter welding times. This is the result of less frictional heating, limiting plastic deformation during the plunging stage, and is consistent with the findings of Cao et al. [16]. A marked difference can be seen in the hook region for welds produced with the chamfered shoulder (Fig. 5d–f, where no hook formed at any welding time and the seam between the top and bottom sheet joins the SZ at a normal angle. This is clearly shown in the magnified images of Fig. 5b,e.

This improvement in hook defect behaviour can be attributed to the narrower end-face of the chamfered shoulder (Fig. 4b), allowing it to plunge through the sheets with less plastic deformation.

3.1.2 Interface mixing

The SZ/TMAZ interface is the circumferential region at the outside of the shoulder plunge path, where the displaced material is forced back together with the bulk material during the refill stage. Poor bonding in this region creates a path for crack propagation and leads to reduced joint strength [31–33]. When using the standard shoulder, the quality of the SZ/TMAZ interface was strongly influenced by welding time, with shorter times leading to voids and poor consolidation (Fig. 5a–c). In contrast, mixing at the SZ/TMAZ interfaces of welds produced with the chamfered shoulder were not affected by welding time and no voids were present in this region (Fig. 5d–f). These improvements can be attributed to the influence of the chamfer geometry on material flow during the refill stage. As illustrated in Fig. 6, during the refill stage the pin forces the displaced material back into the weld and applies pressure to promote bonding at the lap and SZ/TMAZ interfaces [34, 35].

In the case of the standard shoulder (Fig. 6a), plasticised material must flow around the 90° inner edge of the shoulder tip in order to reach the SZ/TMAZ interface. In longer duration welds, this does not present a problem as higher temperatures and lower deformation rates mean the material can flow more easily [36]. This does not hold true for short welding times where less frictional heat is generated and, consequently, the material's ability to flow is reduced [35]. Under these circumstances, it is difficult for material to flow around the shoulder, hence most of the pin force is applied to the lap interface, rather than the SZ/TMAZ. This is evidenced in Fig. 6a i–ii by the poor mixing and presence of voids at the SZ/TMAZ interface and high-quality bonding at the lap interface. The introduction of the chamfer geometry (Fig. 6b) eases the flow of material and redirects more of the pressure applied by the pin from the lap interface towards the SZ/TMAZ interface, leading to improved mixing and elimination of voids in this region (Fig. 6b i). However, a consequence of this effect is a reduction of pressure applied at the lap interface, leading to a lack of mixing between top and bottom sheets (Fig. 6b ii). While outside the scope of this study, these results suggest that the chamfer angle could be tailored to balance pressure between SZ/TMAZ and lap interfaces for optimal bonding in both regions.

3.1.3 Tunnel defect

Tunnel defects are continuous or intermittent voids that run circumferentially around the weld periphery at the deepest

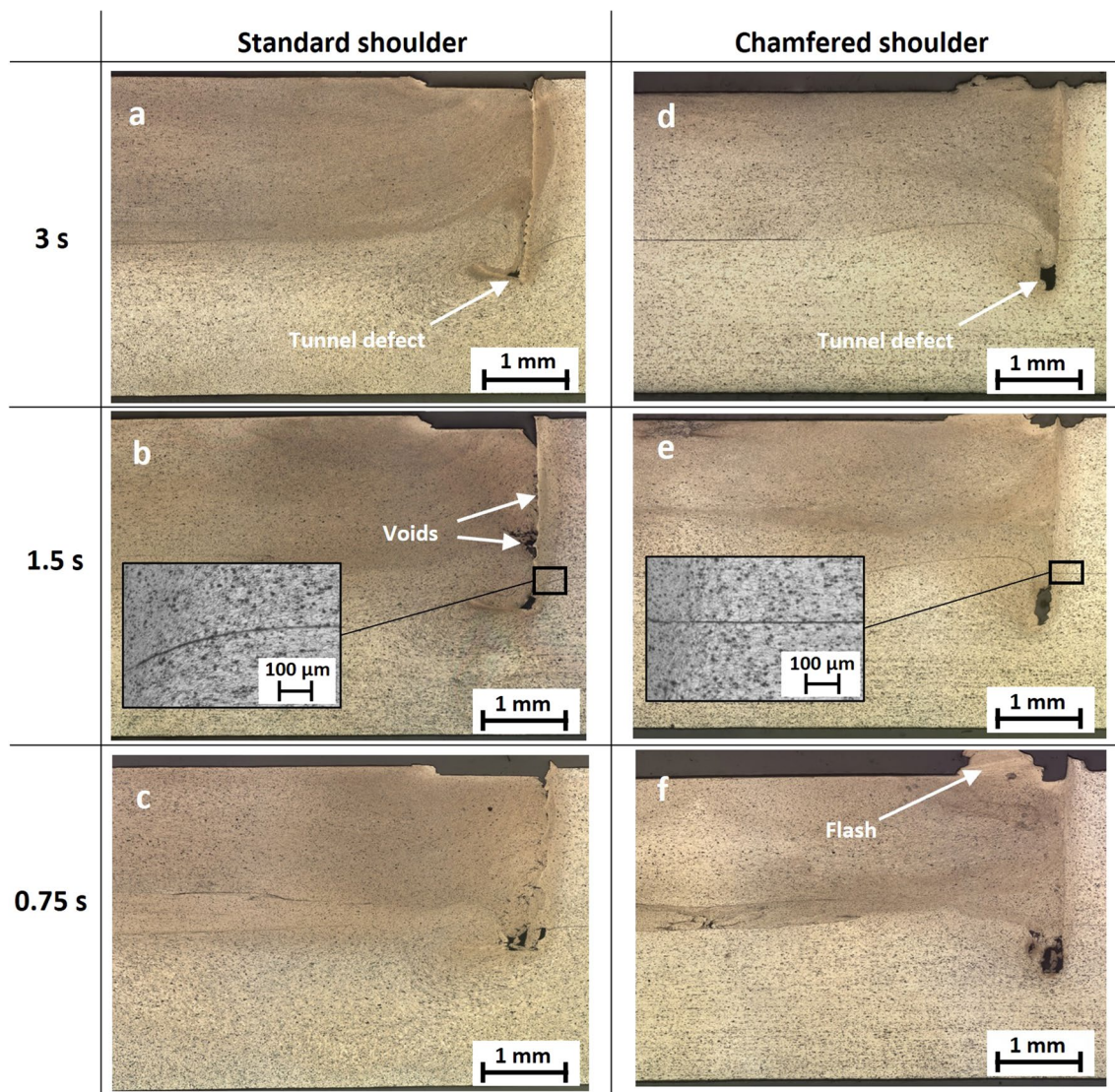


Fig. 5 Micrographs of welds produced at varying weld times, 1500 rpm rotational speed, and 2.25 mm plunge depth using a standard shoulder (a-c) and chamfered shoulder (d-f)

point of the shoulder plunge path [37]. This defect is the result of poor material flowability and is typically associated with insufficient heat input, therefore presents a challenge at short welding times [36, 37]. Figure 5 shows that tunnel defects were present in all welds and were influenced by the shoulder geometry and welding time. The size of the defects increased as welding time decreased, which is consistent with poor material flowability due to reduced heat generation, and is in agreement with the findings of Shen et al. [36]. As a small volume of tool material was removed to create the chamfer profile, a corresponding flash was left on the surface of each weld, as indicated in Fig. 5f. This represents workpiece material that is not refilled back into the weld and, as such, contributes to the larger tunnel defects seen in the chamfered shoulder welds (Fig. 5d-f).

3.2 Weld microstructure

Figure 7 compares micrographs of the SZ and SZ/TMAZ interface of welds produced with standard and chamfered shoulders at 1.5 s welding time. The images are taken from a top-down orientation, 1 mm below the weld surface, as illustrated in Fig. 7a. Within the SZ (Fig. 7b i-ii), grains are refined and equiaxed due to the intense stirring of the tool. Figure 7b iii-iv show the transition from SZ to TMAZ, where the refined grain structure begins to coarsen and become elongated in the direction of the tool rotation, before transitioning into the coarser structure of the bulk material. Grain structure within the SZ was found to be more refined in welds produced with the standard shoulder than with the chamfered shoulder at a given welding time (Fig. 7b i-ii).

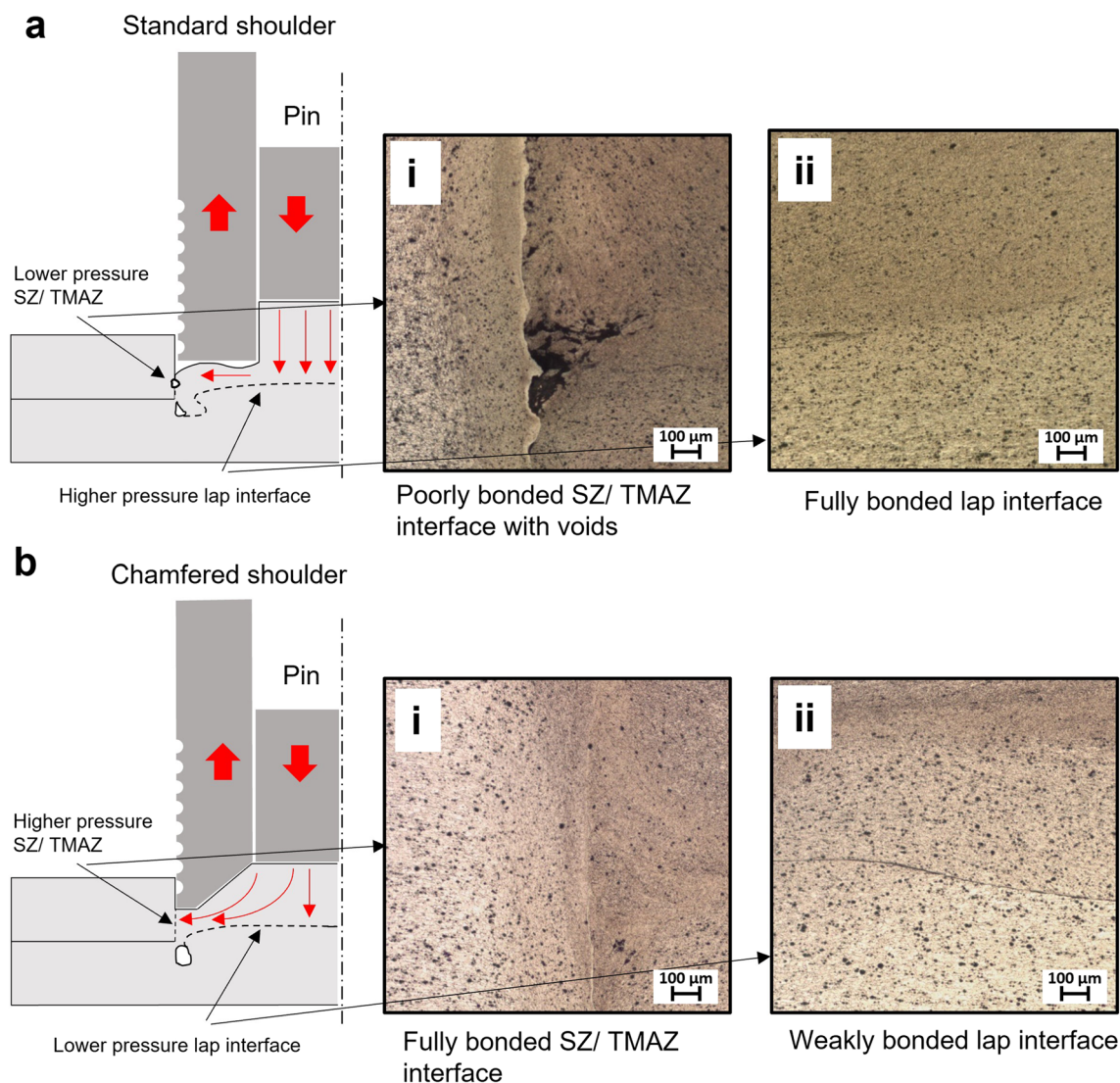


Fig. 6 Material refill behaviour for 1.5 s duration welds using **a)** standard shoulder, **b)** chamfered shoulder

The opposite holds true at the SZ/ TMAZ interface, where grains are more heavily refined in welds produced with the chamfered shoulder. Both of these observations are consistent with the analysis presented in Section 3.1.2, in that the chamfered shoulder redirects more of the pin's refill force towards the weld periphery, leading to more aggressive mixing and grain refinement in this region. Figure 7b iii-iv also reveal that the chamfer reduced the width of the TMAZ by approximately 20%. This can be attributed to the punching effect of the narrower shoulder end-face (Fig. 4) causing less plastic deformation during the plunging stage.

Microhardness maps for welds produced with both shoulder variants at different welding times are presented in Fig. 8. All welds displayed a hardening effect in the SZ region, consistent with intense plastic deformation and the grain refinement shown in Fig. 7. As discussed in Section 3.1.2,

the standard shoulder led to strong mixing at the lap interface but poor mixing at the SZ/ TMAZ interface, whereas the opposite was the case for chamfered shoulder welds. As a result, standard shoulder welds all have a deeper SZ that extends into the bottom sheet. The chamfered shoulder SZs do not extend into the bottom sheet, which is consistent with the lack of mixing at the lap interface observed in Fig. 5.

This hardening behaviour was also influenced by the welding time. At 3 s welding time, both shoulder variants led to similar minimum and maximum hardness of approximately ± 20 HV from that of the base material (140 HV), as shown in Fig. 8a,d. However, a more prominent HAZ is visible for the chamfered shoulder, indicating that higher welding temperatures may have been reached, although further testing is required to confirm this assertion. As welding time is reduced, so too is the

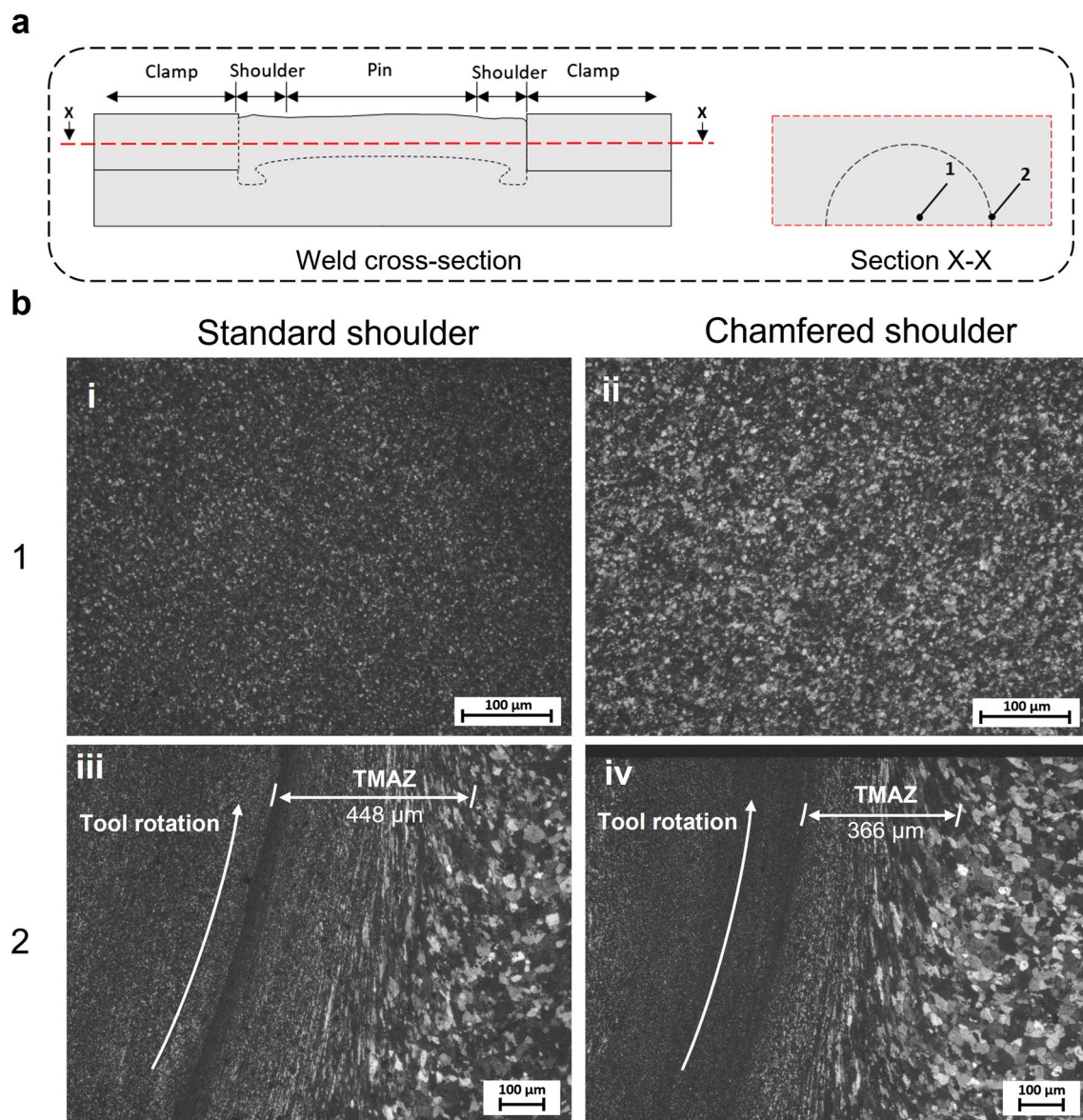


Fig. 7 Micrographs of welds at welding time = 1.5 s, etched with Barker's solution: **a**) diagram of weld and micrograph locations **b**) micrographs within SZ and SZ/TMAZ interface

heat generation and associated thermal effects. This can be seen in all 1.5 s and 0.75 s welds, where no softening is evident to indicate a distinct HAZ.

3.3 Tensile shear testing and failure modes

The results of tensile lap-shear testing are presented in Table 3. While the highest ULSF of 9.05 kN was achieved with the standard shoulder at 3 s welding time, a sharp decrease in strength to 6.45 kN was observed as welding time was reduced to 1.5 s, along with a further drop to 6.06 kN at 0.75 s. This represents a 33% drop in ULSF and

highlights the sensitivity of the standard shoulder to welding time. In contrast, with the chamfered shoulder, ULSF was consistent at 3 s and 1.5 s (≈ 8 kN) and decreased by 10%, (to 7.02 kN) at 0.75 s welding time. This can be attributed to the improved mixing at the SZ/TMAZ interface, discussed in Section 3.1, and supported by the change in failure mode shown in Fig. 10.

Figure 9 compares the results of this study with those of the published RFSSW literature for 2xxx series aluminium alloys, highlighting the positive influence of the chamfered shoulder and that a substantial reduction in welding time is achievable without a significant loss of ULSF.

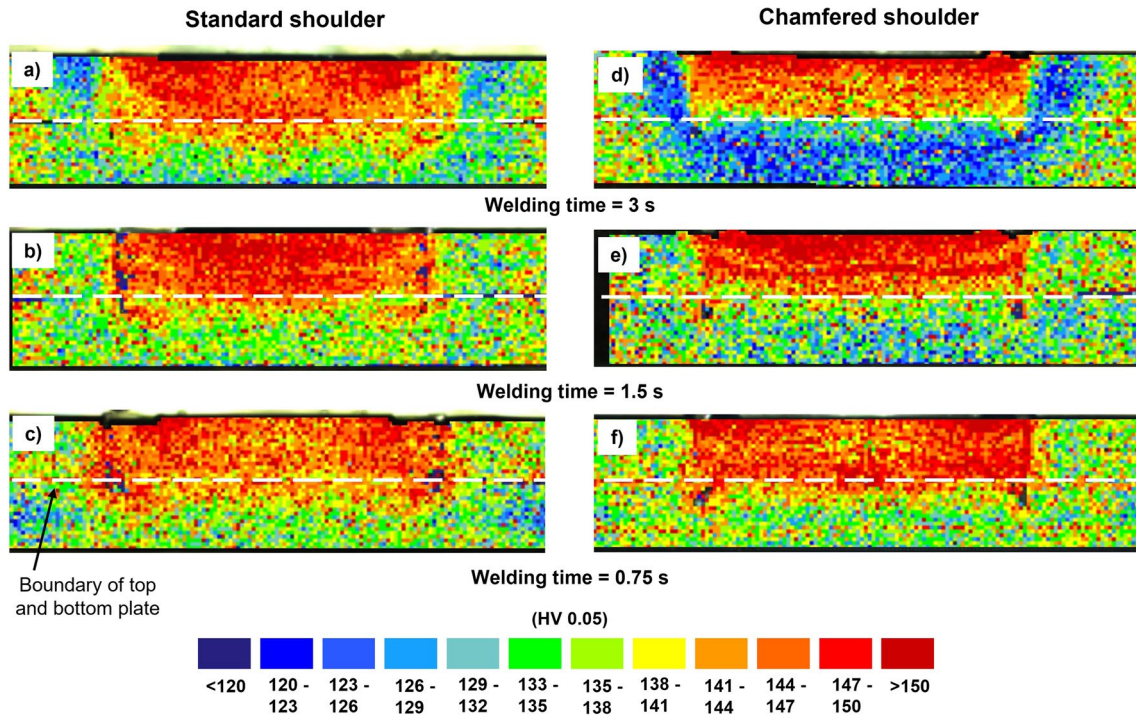
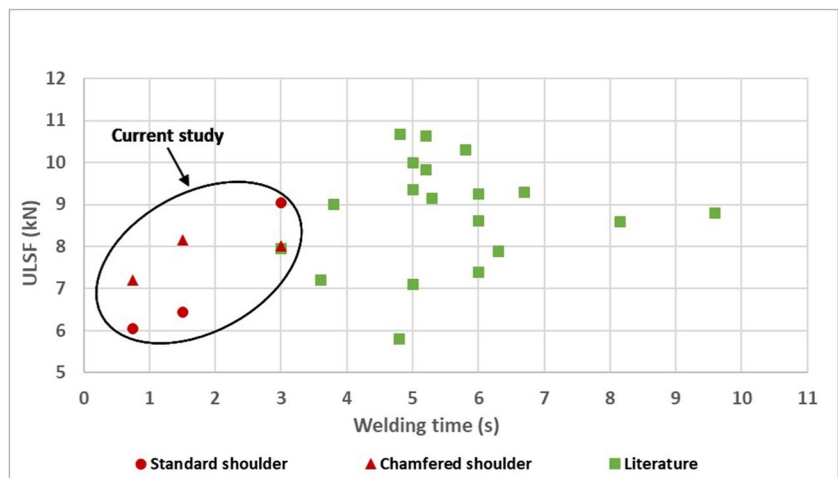


Fig. 8 Hardness profiles for welds produced at 1500 rpm with modified shoulder geometries

Table 3 Results of tensile lap-shear testing

Parameter ID	Shoulder type	Welding time (s)	Lap-shear force (kN)	Standard deviation (kN)	Sample failure mode		
					1	2	3
01	Standard	3	9.05	0.34	PPO	PPO	PPO
02		1.5	6.45	0.55	PPO	PPO	PPO
03		0.75	6.06	0.17	PPO	TWS	PPO
04	Chamfered	3	8.01	0.14	TWS	TWS	TWS
05		1.5	8.16	0.11	TWS	TWS	TWS
06		0.75	7.20	0.27	PPO	PPO	PPO

Fig. 9 Comparison of ULSF results from this study with published literature for RFSSW joints of 2xxx series aluminium alloys [5, 10, 17, 26–28, 33, 34, 38–50]



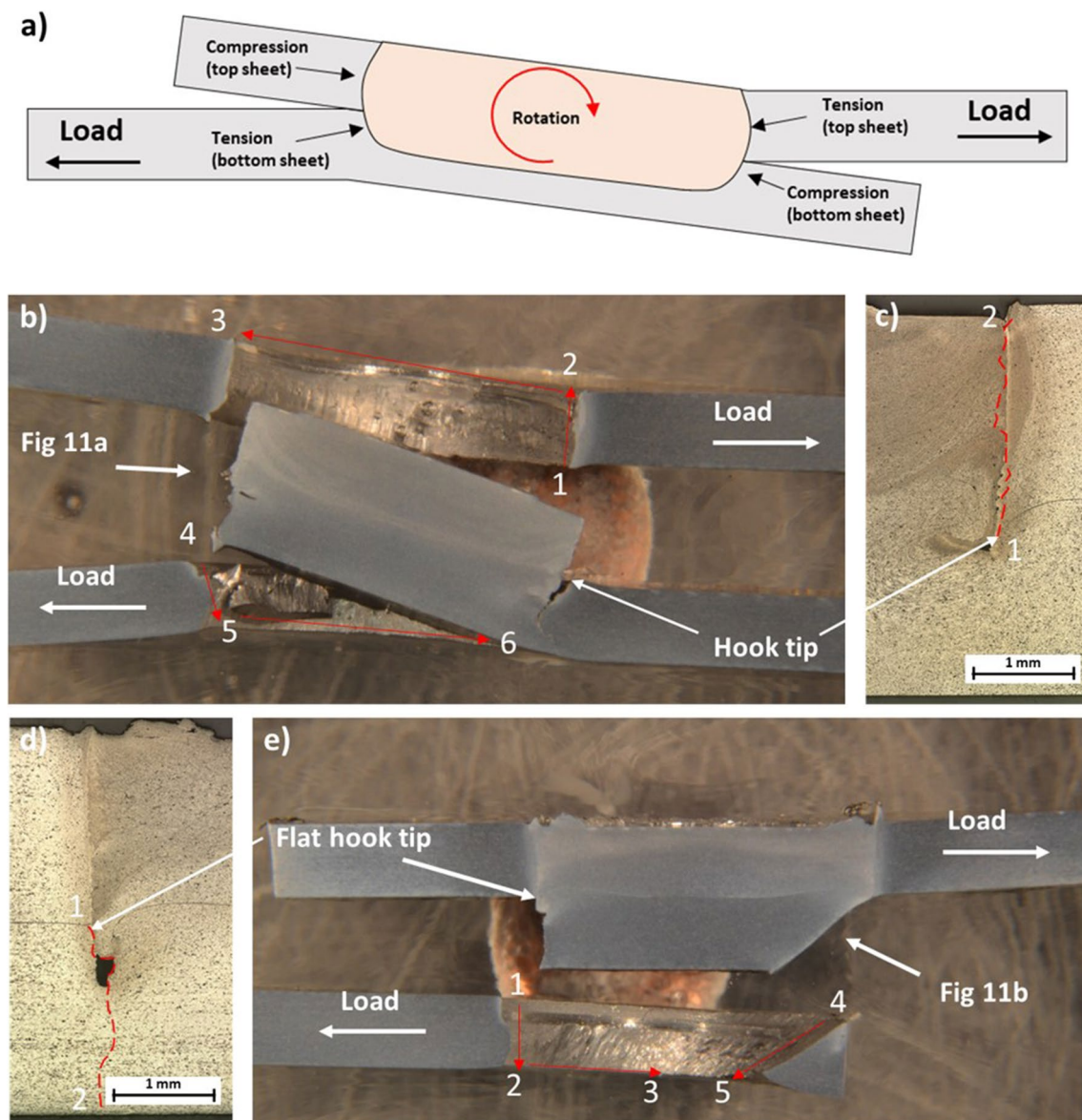


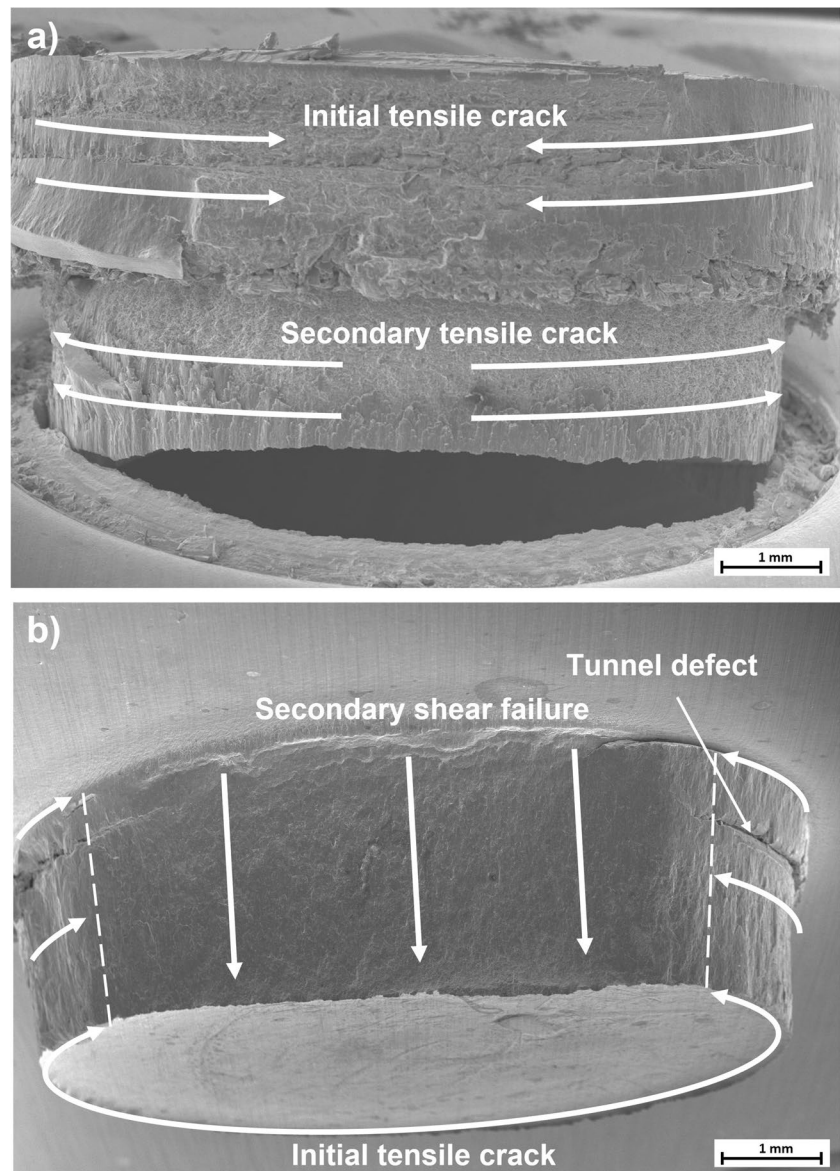
Fig. 10 Failure modes of RFSSW joints made at 3 s welding time, 1500 rpm rotational speed, and 2.25 mm plunge depth **a)** joint configuration during tensile lap-shear testing **b-c)** PPO failure, **d-e)** TWS failure

Post-tensile testing fractography revealed two modes of failure that have been reported extensively in the literature [5, 9, 34, 38, 51, 52]: plug pull-out (PPO) (Fig. 10b-c) and 45° shear through the bottom sheet (TWS) (Fig. 10d-e). PPO failure occurred in almost all welds produced with the standard shoulder, as well as in the 0.75 s welds produced with the chamfered shoulder. Welds produced at 1.5 s and 3 s welding time with the chamfered shoulder all failed by TWS.

The loading of welds during lap-shear testing is complex, with different regions in tension and compression, as illustrated in Fig. 10a. During PPO failures, a crack initiates at the

hook tip in the tensile region of the top sheet and propagates upwards through the SZ/ TMAZ interface and around the weld periphery, moving through points 1, 2 and 3 as indicated in Fig. 10b [52]. The offset loading of the lap configuration also causes a rotation about the centre of the joint, allowing a secondary crack to open at the hook tip in the tensile region of the bottom sheet (point 4). This secondary crack advances downwards, towards the bottom of the weld (point 5) and around the periphery towards point 6, until the weld nugget is pulled completely from one or both sheets [36]. Figure 11a shows the compressive face of the weld nugget from the direction indicated in Fig. 10a after PPO failure has occurred.

Fig. 11 SEM images of **a)** weld nugget after PPO failure **b)** weld nugget after TWS failure through the bottom sheet



In the case of TWS failures through the bottom sheet, the initial fracture begins at the hook tip in the bottom sheet (Fig. 10d-e). Referring to Fig. 10e, the crack travels downwards from the hook at point 1 and into the tunnel defect. The tunnel defect then acts as a stress concentrator, allowing the crack to propagate through the remainder of the bottom sheet to point 2. The crack then moves around the weld periphery towards point 3 until the remaining intact material can no longer support the test load. A secondary failure then begins at the opposing hook tip, shearing rapidly through the path from point 4 to point 5. The SEM image presented in Fig. 11b shows the weld nugget of a TWS failure from the direction indicated in Fig. 10e. The progress made by the initial tensile crack around the weld periphery before shear fracture occurs can be identified by

the disappearance of the tunnel defect, as the shear fracture does not propagate through the tunnel.

These failure modes show that in this study the primary weld characteristic influencing ULSF was the quality of joining at the SZ/ TMAZ interface. With a 3 s welding time, both shoulder variants produced good quality mixing in this region, however the chamfered shoulder welds failed prematurely due to large tunnel defects which led to crack propagation through the bottom sheet. At a shorter welding time of 1.5 s, ULSF dropped significantly for the standard shoulder welds because of poor mixing at the SZ/ TMAZ interface, allowing early PPO failure to occur. Mixing at the SZ/ TMAZ interface remained sufficient for the chamfered shoulder welds because of the redistribution of refill pressure, as illustrated in Fig. 5, and as such ULSF remained constant.

4 Conclusions

This study has investigated the use of a novel axisymmetric shape modification to the shoulder tip of a RFSSW tool, in the form of a 45° chamfer on the shoulder's inner edge. Compared with the standard shoulder, the modified shoulder was shown to influence the refill path of weld material and improve bonding at the SZ/TMAZ interface, leading to higher strength joints at very short welding times of 0.75 s and 1.5 s. However, the presence of the chamfer also caused large tunnel defects and reduced mixing at the lap interface. The following key conclusions can be drawn from this work:

1. The inclusion of a chamfer to the shoulder tip improved bonding and eliminated defects at the SZ/TMAZ interface by easing material flow towards the weld periphery during the refill stage.
2. The quality of bonding at the SZ/ TMAZ interface was more influential to ULSF than bonding at the lap interface.
3. All welds produced with the chamfered shoulder had flat hook geometries, compared with downwards sloping hooks for the standard shoulder. This influence on hook geometry could provide a means of reducing the stress concentration effects associated with large hook heights.
4. The ULSF of welds produced with the chamfered shoulder was less influenced by welding time. Average ULSF of welds produced with the chamfered shoulder varied by only 10% over the tested welding times (3 s to 0.75 s) compared to 33% for the standard shoulder.
5. The chamfered shoulder yielded increases in ULSF of 19% (to 7.2 kN) and 27% (to 8.01 kN) for 0.75 s and 1.5 s welds respectively, compared with the standard shoulder.

Acknowledgements The authors gratefully acknowledge the financial support of the Scottish Association for Metals (charity number SC014102) in partial funding of this work, as well as financial support from the Austrian aviation program “TAKEOFF” (PILOT, grant number 852796, 2018) and BMK—The Austrian Ministry for Climate Action, Environment, Energy, Mobility, Innovation and Technology. The authors would also like to acknowledge Magna for making available the joining equipment used in this work, as well as financial support from the University of Strathclyde and Technical University Graz within the Matched PhD programme framework.

Funding This work was funded in part by the Scottish Association for Metals (charity number SC014102), the Austrian aviation program “TAKEOFF” (PILOT, grant number 852796, 2018) and BMK—The Austrian Ministry for Climate Action, Environment, Energy, Mobility, Innovation and Technology. The authors would also like to acknowledge Magna for use of joining equipment, as well as financial support from the University of Strathclyde and Technical University Graz within the Matched PhD programme framework.

Data availability Data will be made available on request.

Declarations

Competing interests The authors have no competing interests to declare that are relevant to the content of this article.

Open Access This article is licensed under a Creative Commons Attribution 4.0 International License, which permits use, sharing, adaptation, distribution and reproduction in any medium or format, as long as you give appropriate credit to the original author(s) and the source, provide a link to the Creative Commons licence, and indicate if changes were made. The images or other third party material in this article are included in the article's Creative Commons licence, unless indicated otherwise in a credit line to the material. If material is not included in the article's Creative Commons licence and your intended use is not permitted by statutory regulation or exceeds the permitted use, you will need to obtain permission directly from the copyright holder. To view a copy of this licence, visit <http://creativecommons.org/licenses/by/4.0/>.

References

1. Feng XS, Bin Li S, Tang LN, Wang HM (2020) Refill Friction Stir Spot Welding of Similar and Dissimilar Alloys: A Review. *Acta Metall Sin English Lett* 33:30–42. <https://doi.org/10.1007/s40195-019-00982-4>
2. US Department of Transportation (2018) Advisory Circular: Corrosion Control for Aircraft
3. Hosseini SA, Abdollah-zadeh A, Naffakh-Moosavy H, Mehri A (2019) Elimination of hot cracking in the electron beam welding of AA2024-T351 by controlling the welding speed and heat input. *J Manuf Process* 46:147–158. <https://doi.org/10.1016/j.jmapro.2019.09.003>
4. Suryanarayanan R, Sridhar VG (2020) Studies on the influence of process parameters in friction stir spot welded joints - A review. *Mater Today Proc* 37:2695–2702. <https://doi.org/10.1016/j.matpr.2020.08.532>
5. Amancio-Filho ST, Camillo APC, Bergmann L, Dos Santos JF, Kury SE, Machado NGA (2011) Preliminary investigation of the microstructure and mechanical behaviour of 2024 aluminium alloy friction spot welds. *Mater Trans* 52:985–991. <https://doi.org/10.2320/matertrans.L-MZ201126>
6. Zhao Y, Dong C, Wang C, Miao S, Tan J, Yi Y (2020) Microstructures evolution in refill friction stir spot welding of al-zn-mg-cu alloy. *Metals (Basel)* 10:145. <https://doi.org/10.3390/met10010145>
7. Vaneghi AH, Bagheri B, Shamsipur A, Mirsalehi SE, Abdollahzadeh A (2022) Investigations into the formation of intermetallic compounds during pinless friction stir spot welding of AA2024-Zn-pure copper dissimilar joints. *Weld World* 66:2351–2369. <https://doi.org/10.1007/s40194-022-01366-6>
8. Zhao YQ, Liu HJ, Lin Z, Chen SX, Hou JC (2014) Microstructures and mechanical properties of friction spot welded Alclad 7B04-T74 aluminium alloy. *Sci Technol Weld Join* 19:617–622. <https://doi.org/10.1179/1362171814Y.0000000235>
9. Silva BH, Zepon G, Bolfarini C, dos Santos JF (2020) Refill friction stir spot welding of AA6082-T6 alloy: Hook defect formation and its influence on the mechanical properties and fracture behavior. *Mater Sci Eng A* 773:138724. <https://doi.org/10.1016/j.msea.2019.138724>
10. Effertz PS, de Carvalho WS, Guimarães RPM, Saria G, Amancio-Filho ST (2022) Optimization of Refill Friction Stir Spot Welded AA2024-T3 Using Machine Learning. *Front Mater* 9:864187. <https://doi.org/10.3389/fmats.2022.864187>

11. Shen Z, Ding Y, Gerlich AP (2020) Advances in friction stir spot welding. *Crit Rev Solid State Mater Sci* 45:457–534. <https://doi.org/10.1080/10408436.2019.1671799>
12. Zou Y, Li W, Shen Z, Su Y, Yang X (2023) Refill friction stir spot welding of aluminum alloys: State-of-the-art and Perspectives. *Welding World* 67:1853–1885. <https://doi.org/10.1007/s40194-023-01552-0>
13. Gauthier E et al (2014) Numerical modeling of electrode degradation during resistance spot welding using CuCrZr electrodes. *J Mater Eng Perform* 23:1593–1599. <https://doi.org/10.1007/s11665-014-0908-9>
14. Tier MD, Rosendo TS, Mazzaferro JA, Mazzaferro CP, dos Santos JF, Strohaecker TR (2017) The weld interface for friction spot welded 5052 aluminium alloy. *Int J Adv Manuf Technol* 90:267–276. <https://doi.org/10.1007/s00170-016-9370-1>
15. Xu Z, Li Z, Ji S, Zhang L (2018) Refill friction stir spot welding of 5083-O aluminum alloy. *J Mater Sci Technol* 34:878–885. <https://doi.org/10.1016/j.jmst.2017.02.011>
16. Cao JY, Wang M, Kong L, Guo LJ (2016) Hook formation and mechanical properties of friction spot welding in alloy 6061–T6. *J Mater Process Technol* 230:254–262. <https://doi.org/10.1016/j.jmatprotec.2015.11.026>
17. Li G, Zhou L, Luo L, Wu X, Guo N (2019) Microstructural evolution and mechanical properties of refill friction stir spot welded alclad 2A12-T4 aluminum alloy. *J Mater Res Technol* 8:4115–4129. <https://doi.org/10.1016/j.jmrt.2019.07.021>
18. Łogin W, Śliwa RE, Ostrowski R (2022) The influence of modification of the front surface geometry of the Rfssw tool sleeve on the plasticization effect and stirring materials during joining sheets made of Aluminum Alloy 2024. *Arch Metall Mater* 67:1435–1442. <https://doi.org/10.24425/amm.2022.141071>
19. Łogin W, Śliwa RE, Ostrowski R, Andres J (2019) The influence of tool geometry for refill friction stir spot welding (RFSSW) on weld properties during joining thin sheets of aluminum alloys. *Arch Metall Mater* 64:975–981. <https://doi.org/10.24425/amm.2019.129483>
20. Shen Z et al (2021) Interfacial bonding and mechanical properties of al/mg dissimilar refill friction stir spot welds using a grooved tool. *Crystals* 11:429. <https://doi.org/10.3390/cryst11040429>
21. Shen Z et al (2020) Material flow during refill friction stir spot welded dissimilar Al alloys using a grooved tool. *J Manuf Process* 49:260–270. <https://doi.org/10.1016/j.jmapro.2019.11.029>
22. Shen Z, Ding Y, Gopkalo O, Diak B, Gerlich AP (2018) Effects of tool design on the microstructure and mechanical properties of refill friction stir spot welding of dissimilar Al alloys. *J Mater Process Technol* 252:751–759. <https://doi.org/10.1016/j.jmatprotec.2017.10.034>
23. Li Y et al (2023) Effect of tool geometry on hook formation and mechanical properties of refill friction stir spot welding in alclad 2A12-T42 aluminium alloy. *Sci Technol Weld Join* 28:478–487. <https://doi.org/10.1080/13621718.2023.2180203>
24. British Standards Institute (2019) Metallic materials. Tensile testing. Method of test at room temperature. London
25. AMAG rolling GmbH (2006) Inspection certificate (EN 10204)
26. de Castro CC, Plaine AH, de Alcântara NG, dos Santos JF (2018) Taguchi approach for the optimization of refill friction stir spot welding parameters for AA2198-T8 aluminum alloy. *Int J Adv Manuf Technol* 99:1927–1936. <https://doi.org/10.1007/s00170-018-2609-2>
27. Da Silva AAM et al. (2007) Performance evaluation of 2-mm thick alclad AA2024 T3 aluminium alloy friction spot welding. <https://doi.org/10.4271/2007-01-3812>
28. Tier MD et al. (2008) The influence of weld microstructure on mechanical properties of alclad AA2024-T3 Friction Spot Welded. SAE Tech Pap. <https://doi.org/10.4271/2008-01-2287>
29. British Standards Institute (2020) Metallic materials - Vickers hardness test BS EN ISO 6507-4:2018. London
30. Fu B et al (2021) Revealing joining mechanism in refill friction stir spot welding of AZ31 magnesium alloy to galvanized DP600 steel. *Mater Des* 209:109997. <https://doi.org/10.1016/J.MATDES.2021.109997>
31. de Carvalho WS, Vioreanu MC, Lutz MRA, Cipriano GP, Amancio-Filho ST (2021) The influence of tool wear on the mechanical performance of AA6061-T6 refill friction stir spot welds. *Materials (Basel)* 14:7252. <https://doi.org/10.3390/ma14237252>
32. Rosendo T et al (2011) Mechanical and microstructural investigation of friction spot welded AA6181-T4 aluminium alloy. *Mater Des* 32:1094–1100. <https://doi.org/10.1016/j.matdes.2010.11.017>
33. Li Z, Gao S, Ji S, Yue Y, Chai P (2016) Effect of rotational speed on microstructure and mechanical properties of refill friction stir spot welded 2024 Al Alloy. *J Mater Eng Perform* 25:1673–1682. <https://doi.org/10.1007/s11665-016-1999-2>
34. Li Z, Ji S, Ma Y, Chai P, Yue Y, Gao S (2016) Fracture mechanism of refill friction stir spot-welded 2024–T4 aluminum alloy. *Int J Adv Manuf Technol* 86:1925–1932. <https://doi.org/10.1007/s00170-015-8276-7>
35. Ji S, Wang Y, Zhang J, Li Z (2017) Influence of rotating speed on microstructure and peel strength of friction spot welded 2024–T4 aluminum alloy. *Int J Adv Manuf Technol* 90:717–723. <https://doi.org/10.1007/s00170-016-9398-2>
36. Shen Z, Yang X, Zhang Z, Cui L, Li T (2013) Microstructure and failure mechanisms of refill friction stir spot welded 7075–T6 aluminum alloy joints. *Mater Des* 44:476–486. <https://doi.org/10.1016/j.matdes.2012.08.026>
37. Adamus J, Adamus K (2019) The analysis of reasons for defects formation in aluminum joints created using RFSSW technology. *Manuf Lett* 21:35–40. <https://doi.org/10.1016/j.mfglet.2019.08.005>
38. de Sousa Santos P, McAndrew AR, Gandra J, Zhang X (2021) Refill friction stir spot welding of aerospace alloys in the presence of interfacial sealant. *Weld World* 65:1451–1471. <https://doi.org/10.1007/s40194-021-01113-3>
39. Zhang D, Xiong J, Ma Y, Jiang N, Li J (2022) Study of microstructure characteristics and corrosion behavior of 2524 aluminum alloy RFSSW joint. *Mater Charact* 190:112057. <https://doi.org/10.1016/j.matchar.2022.112057>
40. Zou Y et al (2021) The impact of macro/microstructure features on the mechanical properties of refill friction stir spot-welded joints of AA2219 alloy with a large thickness ratio. *Int J Adv Manuf Technol* 112:3093–3103. <https://doi.org/10.1007/s00170-020-06504-2>
41. Schmal C, Meschut G, Buhl N (2019) Joining of high strength aluminum alloys by refill friction stir spot welding (III-1854-18). *Weld World* 63:541–550. <https://doi.org/10.1007/s40194-018-00690-0>
42. Sun G et al (2023) Quality improvement of refill friction stir spot welds in 2A12-T42 aluminum alloy with alclad by adjusting sleeve design. *Int J Adv Manuf Technol* 130:1723–1734. <https://doi.org/10.1007/s00170-023-12834-8>
43. Yue Y, Shi Y, Ji S, Wang Y, Li Z (2017) Effect of sleeve plunge depth on microstructure and mechanical properties of refill friction stir spot welding of 2198 aluminum alloy. *J Mater Eng Perform* 26:5064–5071. <https://doi.org/10.1007/s11665-017-2929-7>
44. Shi Y, Yue Y, Zhang L, Ji S, Wang Y (2018) Refill Friction Stir Spot Welding of 2198–T8 Aluminum Alloy. *Trans Indian Inst Met* 71:139–145. <https://doi.org/10.1007/s12666-017-1146-2>
45. Pieta G, Dos Santos J, Strohaecker TR, Clarke T (2014) Optimization of friction spot welding process parameters for AA2198-T8 sheets. *Mater Manuf Process* 29:934–940. <https://doi.org/10.1080/10426914.2013.811727>
46. Shang Z, Zuo Y, Ji S, Wang Y, Chai P (2021) Joint formation and mechanical properties of 2060 aluminum alloy refill friction stir

- spot welding joint. *Arch Metall Mater* 66:153–161. <https://doi.org/10.24425/amm.2021.134771>
47. Chai P, Wang Y (2019) Effect of Rotational Speed on Microstructure and Mechanical Properties of 2060 Aluminum Alloy RFSSW Joint. *Met Mater Int* 25:1574–1585. <https://doi.org/10.1007/s12540-019-00291-6>
 48. Wang Y, Chai P, Ma H, Cao X, Zhang Y (2020) Formation mechanism and fracture behavior in extra-filling refill friction stir spot weld for Al–Cu–Mg aluminum alloy. *J Mater Sci* 55:358–374. <https://doi.org/10.1007/s10853-019-03940-8>
 49. Zou Y et al (2022) Characterizations of dissimilar refill friction stir spot welding 2219 aluminum alloy joints of unequal thickness. *J Manuf Process* 79:91–101. <https://doi.org/10.1016/J.JMAPRO.2022.04.062>
 50. Wang Y, Chai P (2020) Effects of welding parameters on micro-junction structure and fracture behavior of refill friction stir spot welded joints for 2060 aluminum alloys. *Weld World* 64:2033–2051. <https://doi.org/10.1007/s40194-020-00981-5>
 51. Fritsche S, Draper J, Toumpis A, Galloway A, Amancio-Filho ST (2022) Refill friction stir spot welding of AlSi10Mg alloy produced by laser powder bed fusion to wrought AA7075-T6 alloy. *Manuf Lett* 34:78–81. <https://doi.org/10.1016/j.mfglet.2022.09.010>
 52. Zou Y et al (2021) Formability and mechanical property of refill friction stir spot-welded joints. *Weld World* 65:899–907. <https://doi.org/10.1007/s40194-020-01056-1>

Publisher's Note Springer Nature remains neutral with regard to jurisdictional claims in published maps and institutional affiliations.